





Electron spin secluded inside a bottom-up assembled standing metal-molecule nanostructure

Taner Esat ^{1,2,*}, Markus Ternes ^{1,2,3}, Ruslan Temirov ^{1,2,4} and F. Stefan Tautz ^{1,2,5}

¹Peter Grünberg Institute (PGI-3), Forschungszentrum Jülich, 52425 Jülich, Germany

²Jülich Aachen Research Alliance (JARA), Fundamentals of Future Information Technology, 52425 Jülich, Germany

³Institute of Physics II B, RWTH Aachen University, 52074 Aachen, Germany

⁴Institute of Physics II, University of Cologne, 50937 Cologne, Germany

⁵Experimental Physics IV A, RWTH Aachen University, 52074 Aachen, Germany



(Received 27 January 2023; revised 26 July 2023; accepted 21 August 2023; published 20 September 2023)

Artificial nanostructures, fabricated by placing atoms or molecules as building blocks in well-defined positions, are a powerful platform in which quantum effects can be studied and exploited. In particular, they offer the opportunity to reduce the electronic interaction between large aromatic molecules and the underlying metallic substrate, if the manipulation capabilities of scanning tunneling microscopy to lift the molecule into an upright geometry on a pedestal of two metal atoms are used. Here, we report a strategy to study this interaction by investigating the Kondo effect. Measurements at millikelvin temperatures and in magnetic fields reveal that this bottom-up assembled standing metal-molecule nanostructure has an $S = 1/2$ spin which is screened by substrate electrons, resulting in a Kondo temperature of only 291 ± 13 mK. We extract its Landé g factor and its exchange coupling $J\rho$ to the substrate, using a third-order perturbation theory in the weak-coupling and high-field regimes. We also show that the interaction between the scanning tunneling microscope tip and the molecule can tune the exchange coupling.

DOI: [10.1103/PhysRevResearch.5.033200](https://doi.org/10.1103/PhysRevResearch.5.033200)

I. INTRODUCTION

On the way to spin qubits based on single atoms or molecules, it is essential to minimize the coupling of their spins to the environment, since the latter leads to decoherence [1]. The scanning tunneling microscope (STM) is an ideal tool to study quantum properties of nanoscale structures, because it not only allows the magnetic states of individual atoms and molecules to be read out [2] and coherently controlled [3–5], but also enables one to change the environment controllably. Its ability to arrange atoms and molecules on surfaces with atomic precision permits the fabrication of unprecedented artificial nanostructures [6,7]. Hence the STM can be used to fabricate multiple absolutely identical qubits [8] from individual atoms and molecules, which can be arranged and coupled with each other as desired. This ultimate structural control offers clear advantages over mesoscopic qubits.

Magnetic atoms and molecules with spin-degenerate ground states on metallic surfaces typically show the Kondo effect: The spin degree of freedom is quenched at temperatures below the Kondo temperature T_K by the formation of a many-electron singlet state with the bath electrons [9,10].

Because T_K depends on the coupling of the spin degree of freedom with the metal, the Kondo effect can be used to gauge the interaction of the magnetic atom or molecule with the metallic environment. The strong hybridization of the d orbitals of magnetic atoms with metals leads to T_K of typically 40–300 K [11]. For magnetic molecules, on the other hand, Kondo temperatures of only a few kelvins have been observed [12–14], which can be explained by the weaker hybridization of the molecular orbitals with the substrate, or the shielding of the magnetic atoms within the molecules by the surrounding ligands. Long spin relaxation times T_1 of several hundred nanoseconds up to days [15,16] and dephasing times T_2 in the nanosecond range [3–5] were so far only achieved for atoms and molecules decoupled from the metal by an atomically thin insulating layer. The presence of decoupling layers has also resulted in a significant reduction of T_K to a few kelvins for magnetic atoms [17,18].

Here, we show that exploiting the third dimension for the bottom-up assembly of standing metal-molecule nanostructures offers an alternative approach to tune the substrate coupling of a spin degree of freedom in a molecule. Specifically, we show that for a single 3,4,9,10-perylenetetracarboxylic dianhydride (PTCDA) molecule in the standing configuration on a pedestal of two Ag adatoms [Fig. 1(a)], the coupling with the Ag(111) surface is drastically reduced compared with flat-lying PTCDA while at the same time it can be tuned by stretching the bond between the molecule and surface. We report the fabrication of an $S = 1/2$ spin nanostructure based on this strategy, with a very weak substrate coupling resulting in a T_K of only 291 ± 13 mK. To our knowledge, no smaller T_K has been reported for adsorbates on metal surfaces

*Corresponding author: t.esat@fz-juelich.de

Published by the American Physical Society under the terms of the [Creative Commons Attribution 4.0 International license](https://creativecommons.org/licenses/by/4.0/). Further distribution of this work must maintain attribution to the author(s) and the published article's title, journal citation, and DOI.

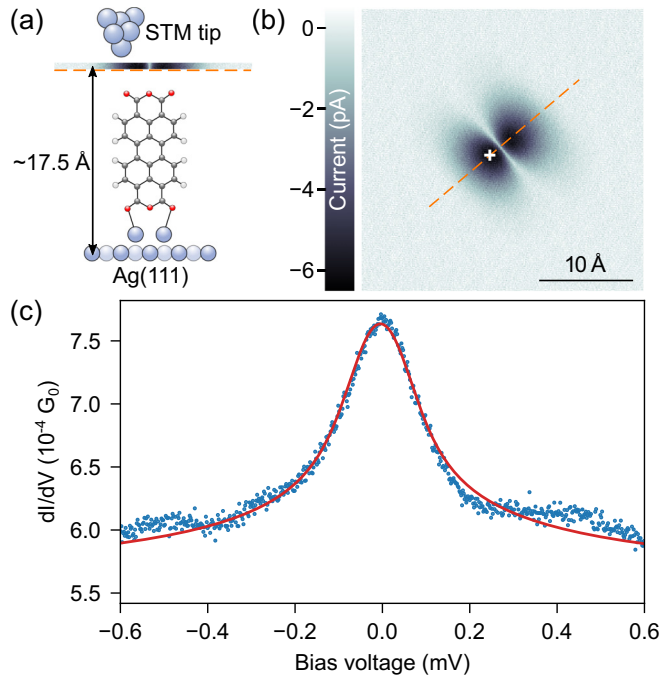


FIG. 1. (a) Schematic view of a standing PTCDA + 2Ag nanostructure on the Ag(111) surface, including the STM tip above the molecule. The bar shows the tunneling current I_T measured above the standing nanostructure at constant height. The white, gray, and red spheres indicate hydrogen, carbon, and oxygen atoms, respectively, of PTCDA. (b) Constant-height STM image above a standing nanostructure recorded at a tip height of $z \simeq 17.5$ Å above the surface. The bias voltage was $V = -50$ mV. The white cross marks the location where the dI/dV conductance spectra were measured. The molecular plane is indicated by the dashed orange line. (c) dI/dV conductance spectrum (blue) on a standing metal-molecule nanostructure measured at $T = 30$ mK and $B = 0$ T ($I_T = 45$ pA, $V = -1$ mV, $V_{\text{mod}} = 50$ μ V). The red curve shows the fit based on the Frota function (see text for details). The spectrum is shown in units of the conductance quantum $G_0 = \frac{2e}{h}$.

to date. Comparably low T_K have so far only been found in mesoscopic quantum dots [19,20].

II. EXPERIMENTAL DETAILS

The Ag(111) surface was prepared in ultrahigh vacuum by repeated Ar^+ sputtering and heating at 800 K. A small coverage of PTCDA molecules was evaporated onto clean Ag(111) at room temperature from a custom-built Knudsen cell. Next, the sample was flashed at 480 K for 2 min before being cooled down to 100 K and transferred to the STM. All experiments were performed in the Jülich Quantum Microscope [21], a millikelvin STM which uses the adiabatic demagnetization of a magnetocaloric material to reach temperatures between 30 mK and 1 K. Differential conductance (dI/dV) spectra were measured using conventional lock-in techniques with the STM feedback loop switched off and an ac modulation amplitude $V_{\text{mod}} = 20$ –100 μ V and frequency $f_{\text{mod}} = 187$ Hz.

The standing PTCDA + 2Ag nanostructure was fabricated on Ag(111) in three steps by controlled manipulation with the STM tip [22]. First, two single Ag atoms were

attached to the two carboxylic oxygens on one side of the flat-lying molecule by lateral manipulation. Then, one of the carboxylic oxygens on the opposite side was tip-contacted, and PTCDA was pulled up on a curved trajectory until it stood upright. The tip was then moved straight up until the bond between molecule and tip broke, leaving the molecule standing on the two adatoms [22]. The stability of the standing metal-molecule nanostructure arises from the balance between local covalent and long-range van der Waals interactions [23,24].

III. RESULTS AND DISCUSSION

In constant-height STM images, the standing metal-molecule nanostructure exhibits two features distributed symmetrically around the plane of the molecule [dashed orange line in Fig. 1(b)] and separated by a nodal plane perpendicular to the latter [Fig. 1(b)]. The two features coincide with the positions where the interaction with the tip is most pronounced [22]. It is interesting that the node of the π orbital in the plane of the molecule is not resolved. In the standing configuration, the overlap between the surface wave functions and the lowest unoccupied molecular orbital (LUMO) is weak, because the lobes of the π orbital are oriented perpendicular to the plane of the molecule. This allows the standing nanostructure to function as a quantum dot and coherent field emitter [22].

A. Kondo effect in the standing metal-molecule nanostructure

At millikelvin temperatures, a peak at zero bias appears in the dI/dV spectrum [Fig. 1(c)]. In fact, due to the dynamical Coulomb blockade (DCB) we additionally observe a dip at zero bias [25]. We have corrected all dI/dV spectra for the DCB dip (see Appendix A). Previous studies have hinted that the LUMO of the standing metal-molecule nanostructure contains an unpaired electron [22,26]. Therefore it is plausible that the zero-bias peak originates from the Kondo effect. To verify this, we measured dI/dV spectra at different B fields. Already at $B \approx 100$ –120 mT a Zeeman splitting of the zero-bias peak is discernible [Fig. 2(a)]. At higher B , the Kondo effect is completely suppressed, and the spectrum is dominated by the symmetric steps of inelastic spin-flip excitations [Fig. 2(b)].

To extract the Zeeman splitting Δ , the peaks of the numerical derivative d^2I/dV^2 were fitted with Gaussians (see Appendix B). As shown in Figs. 2(c) and 2(d), the spin-flip excitations' energies scale linearly with B . Only close to the critical field B_C , required to initially split the Kondo resonance, does the Zeeman energy rise faster. To extract the Landé g factor, we only consider data points at $B \geq 1$ T [Fig. 2(b)], since the Kondo effect in the strong-coupling regime leads to a renormalization of g [27]. A linear fit $\Delta = g\mu_B B$, where μ_B is the Bohr magneton, yields $g = 2.006 \pm 0.007$. By interpolating the data points at low B , we obtain $B_C = 108 \pm 5$ mT. Using the relation

$$B_C = \frac{1}{2} \frac{k_B T_K}{g\mu_B}, \quad (1)$$

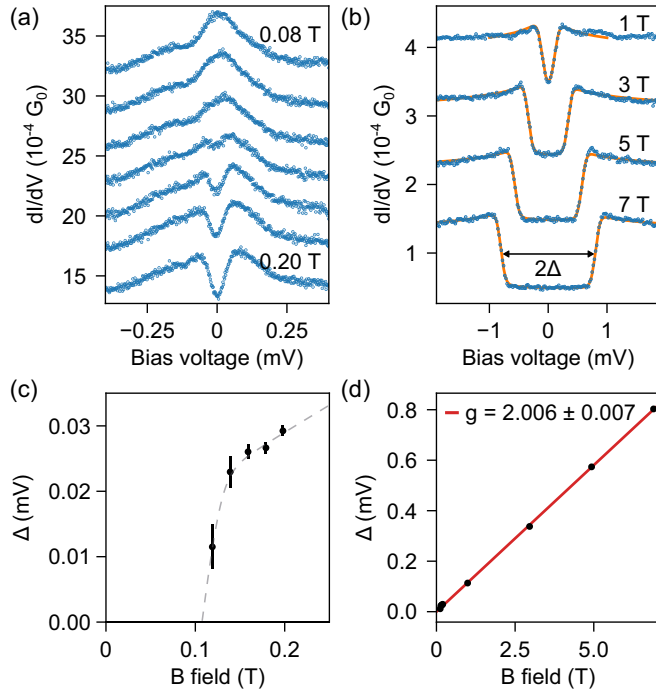


FIG. 2. (a) and (b) dI/dV spectra (blue) on a standing metal-molecule nanostructure, measured at different B fields at $T = 40\text{--}50$ mK [set points in (a) were $I_T = 100$ pA, $V = -1$ mV, $V_{\text{mod}} = 20$ μ V, and set points in (b) were $I_T = 100$ pA, $V = -10$ mV, $V_{\text{mod}} = 100$ μ V]. In (a), the B field was changed in steps of 20 mT. The orange curves in (b) show the fits based on perturbation theory (see text for details). The spectra are vertically displaced by multiples of $3.0 \times 10^{-4}G_0$ with respect to the spectrum measured at 0.2 T in (a) and by multiples of $1.0 \times 10^{-4}G_0$ with respect to the spectrum measured at 7 T in (b) for clarity. (c) and (d) The Zeeman splitting Δ extracted from the dI/dV spectra as a function of B . The gray dashed curve in (c) serves as a guide for the eye. The red line in (d) shows the linear fit for the Zeeman splitting.

valid for $T < 0.25T_K$ [28], this gives an estimate of 291 ± 13 mK for T_K .

An independent estimate of T_K can be obtained from the width Γ_K of the Kondo resonance [Fig. 1(c)]. However, it should be noted that this is only a rough estimate, since Γ_K is related to T_K by a nonuniversal scaling constant [29]. To extract Γ_K , we fitted the Kondo resonance with a Frota line [30]

$$\rho(E)_{\text{Frota}} = \text{Re} \sqrt{\frac{i\Gamma_K}{E - E_0 + i\Gamma_K}}. \quad (2)$$

Additional broadening effects due to the Fermi distribution and the modulation amplitude were taken into account (see Appendix C). The best fit yields $\Gamma_K \simeq 43$ μ V and $T_K = \Gamma_K(2\pi \times 0.103)/k_B \simeq 320$ mK [30], in good agreement with the above estimate from the B dependence.

Previous work has shown that the Kondo temperature of a single PTCDA molecule can be reduced by gradually lifting it from the substrate with the STM tip [31–35] and predicted a Kondo temperature in the nanokelvin range when it is completely detached from the surface. The standing configuration shown in this paper essentially corresponds to the PTCDA on

the tip, but fabricated in an atomically precise manner on the surface. Interestingly, our experimental findings differ significantly from the predicted Kondo temperatures, suggesting that neither the conventional Kondo model nor the single-impurity Anderson model is sufficient to describe the physics at least in this standing nanostructure.

The features in the dI/dV spectrum at approximately ± 0.25 and ± 0.55 mV [Figs. 1(c) and 5] are in a similar energy range to that previously assigned to vibrations of the standing metal-molecule nanostructure [23]. Due to the different tunneling set point, the presence of spin excitations, and the different abscissa and ordinate axes, the vibrational features cannot be resolved in the data for high magnetic fields. Note that a strong electron-vibrational coupling can also lead to a further decrease in T_K [36].

B. Interaction of the localized spin with its environment

The low T_K of the standing nanostructure in conjunction with the millikelvin base temperature and high energy resolution of our STM enables us to quantitatively describe the exchange coupling of the localized spin to its environment as a function of T and B . For this purpose, we employ the Anderson-Appelbaum model [37–39] and calculate the tunneling conductance from the Kondo Hamiltonian in a perturbative approach that includes processes up to third order in the exchange interaction J [40]. The model includes the spin-spin exchange scattering ($t_{TS} \hat{\sigma}_t \cdot \hat{S}$) and potential scattering ($t_{TS} U$) of tunneling electrons (spin $\hat{\sigma}_t$) with the local spin \hat{S} in the nanostructure. It also takes into account the spin-spin exchange scattering $J\rho \hat{\sigma}_s \cdot \hat{S}$ between the substrate electrons (spin $\hat{\sigma}_s$) and the local spin, where ρ denotes the substrate's electron density at the Fermi energy. This approach provides the correct description if the local spin is predominantly coupled to one of the electrodes (here the substrate), the system is in equilibrium (limit of small bias voltages), and the system is in the weak-coupling ($T \gtrsim T_K$) or high-field ($B \gtrsim k_B T_K$) regimes. We performed least-squares fits and extracted the dimensionless coupling strength $J\rho$ and the g factor of the local spin.

Before focusing on the T dependence, we first examine the influence of the B field on $J\rho$ at 50 mK [Fig. 2(b)]. As B increases, the height of the peak structures on top of the spin-flip excitation steps decreases. Since these peak heights are proportional to $J\rho$ [40], this indicates that $|J\rho|$ decreases with increasing B . This is evident in Fig. 3(a), where the fitted $J\rho$ is plotted versus B . It may seem surprising that one still observes a coupling between the local and itinerant spins at high B . This behavior is, however, in good agreement with numerical renormalization group calculations for an $S = 1/2$ Kondo impurity at finite T and B [28], where it was shown that the intensity of the split Kondo resonance varies even if $\mu_B B/k_B T_K \gg 1$, which corresponds to the present situation. Thus, even at high B we have access to bias-driven Kondo correlations whose gradual emergence at decreasing T drives $|J\rho|$ up.

This behavior can be readily observed in T -dependent data for constant $B = 7$ T [Fig. 3(b)]. The fits reveal that $|J\rho|$ increases with decreasing T [Fig. 3(c)]. For $B = 0$, an increase of $|J\rho|$ would signal the progressive breakdown of

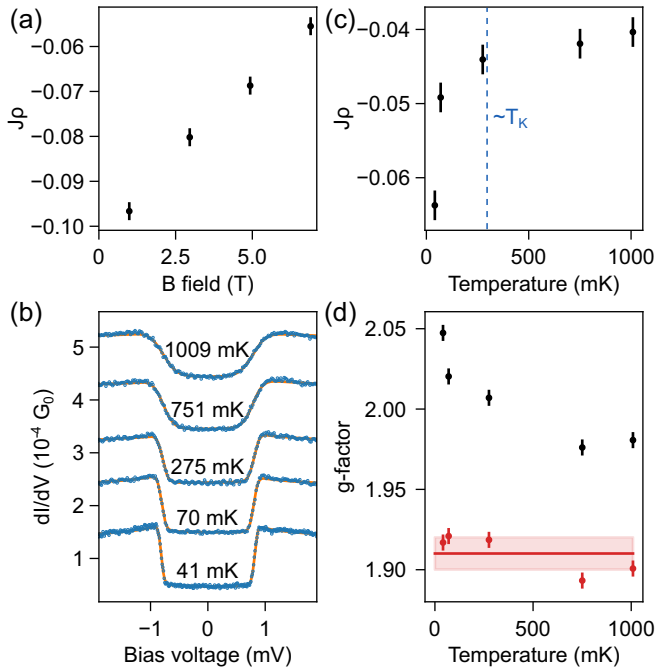


FIG. 3. (a) Coupling strength $J\rho$ as extracted from the fits in Fig. 2(b) as a function of B field. (b) dI/dV spectra (blue) on a standing metal-molecule nanostructure, measured at different temperatures in an external field $B = 7$ T ($I_T = 100$ pA, $V = -10$ mV, $V_{\text{mod}} = 100$ μ V). The orange curves show the fits based on perturbation theory (see text for details). The spectra are vertically displaced by multiples of $1.0 \times 10^{-4} G_0$ with respect to the spectrum at 41 mK for clarity. (c) Coupling strength $J\rho$ as extracted from the fits as a function of temperature. The dashed blue line indicates the Kondo energy scale T_K as determined from the B -field data of Fig. 2. (d) Landé g factor estimated from the fits in (b) (black) and the effective g factor g_{eff} after taking into account renormalization effects due to the exchange interaction (red). The red line illustrates a linear fit, and the red shaded area illustrates the corresponding confidence interval.

the perturbation approach, yielding a divergence of $J\rho$ and the crossover into the Kondo singlet as the new ground state [9,10]. However, here we are in the high-field regime and therefore will not reach the Kondo ground state even in the limit $T \rightarrow 0$. We note that the temperature range in which the perturbation theory starts to collapse [Fig. 3(c)] agrees very well with the Kondo energy scale of 291 ± 13 mK as derived from the B -field behavior at $T < T_K$. For the fitted g factor in Fig. 3(d) we also see a strong decrease with increasing T . This can be attributed to energy renormalization [41]. Taking this into account, we obtain $g_{\text{eff}} = g(T) \times (1 + J\rho(T)) \approx 1.91 \pm 0.01$, which has no T dependence. Note that the deviation of the g factors from the B -dependent measurements in Fig. 2(d) and from the perturbative approach is $\lesssim 6\%$.

We now explore the possibility of tuning the exchange coupling mechanically. The standing metal-molecule nanostructure is susceptible to attractive forces from the tip, allowing controlled tilts, translations, and rotations [22]. If it was possible to tune the vertical distance of the standing nanostructure from the surface with attractive forces from the STM tip, it might also be possible to tune $J\rho$. To in-

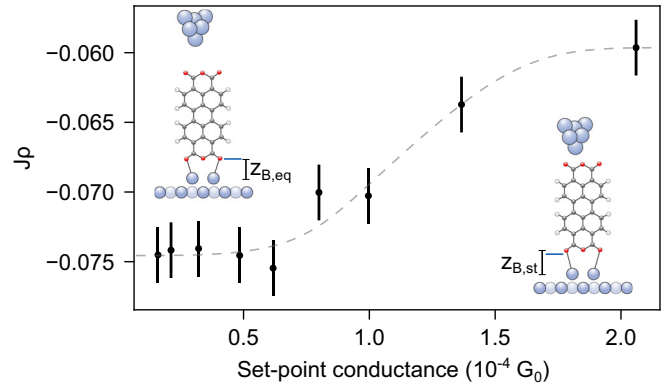


FIG. 4. Coupling strength $J\rho$ as extracted from the fits of dI/dV spectra on a standing metal-molecule nanostructure that were measured for different set-point conductances at $T = 40$ – 50 mK and an external field of $B = 7$ T. The tip was initially stabilized at $I_T = 100$ pA and $V = -6$ mV and then moved up by 1 \AA in steps of 0.1 \AA . The gray dashed curve serves as a guide for the eye. Insets show schematically how the PTCDA molecule is pulled up by the tip.

vestigate this possibility, we measured dI/dV spectra at $B = 7$ T and $T \simeq 45$ mK for different set-point conductances G , corresponding to different distances between the tip and the standing metal-molecule nanostructure. In Fig. 4 the fitted $J\rho$ are plotted as a function of G . For $G \leq 0.6 \times 10^{-4} G_0$, the coupling is constant at $(J\rho)_{\text{eq}} \simeq -0.075$. With increasing G , $|J\rho|$ decreases and reaches $(J\rho)_{\text{st}} \simeq -0.060$ for the highest G . Measurements at even smaller distances are not feasible, because the large tunnel currents frequently induce sudden 30° rotations of the standing nanostructure around its vertical axis. Since we know that there are attractive forces acting between the molecule and the tip [22,23], we interpret the decreasing $|J\rho|$ as the result of an increased distance of the standing metal-molecule nanostructure from the surface. Assuming that the exchange interaction scales exponentially with the bond distance z_B [42], $J(z_B) \propto \exp(-z_B/d_{\text{ex}})$, the vertical relaxation Δz_B of the bond between the standing nanostructure and the surface can be estimated. For a typical decay length $d_{\text{ex}} \simeq 0.4$ \AA [42], we obtain $\Delta z_B = d_{\text{ex}} \ln(J_{\text{eq}}/J_{\text{st}}) \simeq 0.09$ \AA between the smallest and the largest G in Fig. 4.

IV. CONCLUSION

In conclusion, we have shown that in the standing configuration the exchange coupling between the spin degree of freedom of PTCDA within the assembled nanostructure and the Ag(111) surface is strongly reduced compared with the situation for the flat-lying molecule. At $B = 0$ we observed a Kondo resonance with a width of only $\Gamma_K \simeq 43$ μ V at an experimental temperature of $T = 30$ mK. B -field-dependent measurements showed that the standing metal-molecule nanostructure is an $S = 1/2$ system with a critical field of $B_C = 108 \pm 5$ mT. This corresponds to a Kondo temperature of only $T_K = 291 \pm 13$ mK. Interestingly, this differs significantly from the predicted Kondo temperatures of a few nanokelvins for single PTCDA molecules lifted completely from the surface with the STM tip [31–35]. Finally, we note that the standing metal-molecule nanostructure, when

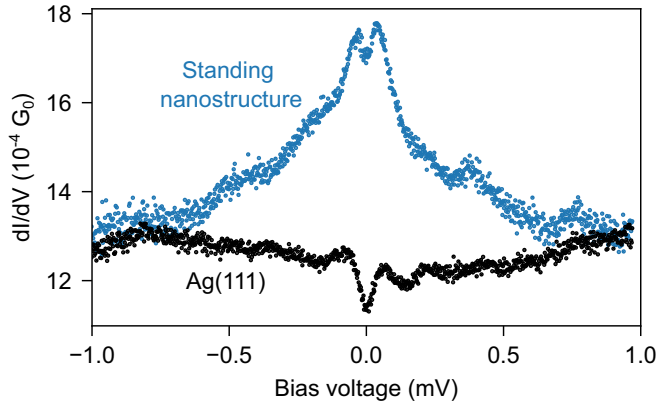


FIG. 5. dI/dV conductance spectra on a standing metal-molecule nanostructure (blue) and on the Ag(111) surface (black) measured at $T = 40\text{--}50$ mK ($V_{\text{mod}} = 20$ μV). The tip was stabilized at $I_T = 100$ pA and $V = -1$ mV. The spectrum on the standing nanostructure corresponds to the spectrum in Fig. 2(a) at $B = 80$ mT.

prepared on the tip, could be employed as a magnetic field sensor on the atomic scale because of its spin properties [13,43–45], in addition to being a sensor of electric surface potentials, in which capacity it has already been used [46,47].

ACKNOWLEDGMENTS

We thank F. B. Anders (TU Dortmund) for fruitful discussions. The authors acknowledge financial support from the German Federal Ministry of Education and Research through the funding program “Quantum Technologies - From Basic Research to Market,” under Q-NL (Projects No. 13N16032 and No. 13N16046). M.T. acknowledges funding from the Heisenberg Program (TE 833/2-1) of the Deutsche Forschungsgemeinschaft (DFG). F.S.T. acknowledges funding from the DFG through SFB 1083 “Structure and Dynamics of Internal Interfaces” (223848855-SFB 1083).

APPENDIX A: DYNAMICAL COULOMB BLOCKADE AT MILLIKELVIN TEMPERATURES

The dynamical Coulomb blockade (DCB) can be observed in the scanning tunneling microscope (STM) at very low temperatures. It results from the inelastic interaction of the tunneling electrons with the electromagnetic environment in which the junction is embedded [48]. In the differential conductance (dI/dV) spectra, it manifests itself as a dip at zero bias [25,49]. In the Jülich Quantum Microscope [21] we typically observe the DCB at temperatures $\lesssim 250$ mK. As can be seen in Fig. 5, the DCB dip is clearly evident in the dI/dV spectra on the standing metal-molecule nanostructure as well as on the Ag(111) surface. We have removed the DCB dip from all dI/dV spectra on the standing nanostructure. For this purpose, we scaled the dI/dV spectrum that was measured on the Ag(111) surface to the background conductance of the respective dI/dV spectrum on the standing nanostructure. Afterwards, we divided the dI/dV spectrum on the standing nanostructure by the spectrum taken on the Ag surface. Finally, we rescaled the obtained dI/dV spectrum back to the original background conductance on the standing nanostructure.

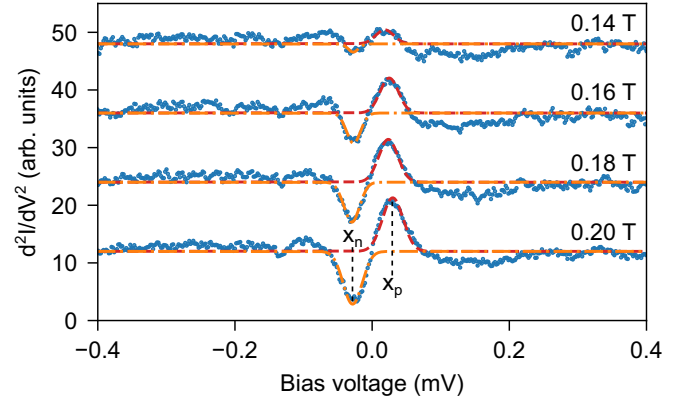


FIG. 6. d^2I/dV^2 spectra (blue) on a standing metal-molecule nanostructure after applying a second-order Savitzky-Golay filter to the dI/dV spectra and calculating the numerical derivative. These data correspond to the dI/dV spectra in Fig. 2(a). The red (orange) dashed curves illustrate the Gaussian fits to the peaks at positive (negative) bias voltage. The spectra are vertically displaced for clarity.

ture. It should be noted that this approach is justified since we measured our dI/dV spectra at low set-point conductances. In the range $<0.2G_0$, different tunneling paths do not affect the shape of the DCB [49], i.e., it is identical on the bare Ag(111) and on the standing nanostructure.

APPENDIX B: DETERMINATION OF THE ZEEMAN ENERGY

In order to extract the precise energy of the Zeeman splitting Δ , we first smoothed the dI/dV spectra measured on the standing metal-molecule nanostructure with a second-order Savitzky-Golay filter, which performs a polynomial fit on a sliding window. To avoid filtering out meaningful signals from the dI/dV spectra, we used a sliding window of only 50 μV width. Afterwards, we calculated the numerical derivative of the dI/dV spectra, i.e., d^2I/dV^2 . In the d^2I/dV^2 spectra, the peaks correspond to the steepest slope of the steps arising from inelastic spin-flip excitations in the dI/dV spectra. To determine the exact position x_p (x_n) of the peaks, we fitted them at positive (negative) bias voltage with a Gaussian. Figure 6 shows the resulting fits for the data shown in Fig. 2(a) as an example. Finally, we calculated the Zeeman energy as $\Delta = (|x_n| + |x_p|)/2$.

APPENDIX C: FITTING OF THE KONDO RESONANCE

To extract the intrinsic width of the Kondo resonance, broadening effects due to temperature and the modulation amplitude of the lock-in amplifier must be taken into account [50]. For this reason, before fitting to the Kondo resonance, we convolved the Frota function both with the derivative of the Fermi-Dirac distribution

$$X_T(\epsilon) = \frac{\beta}{4 \cosh^2(\beta\epsilon/2)} \quad (\text{C1})$$

with $\beta = 1/k_B T$, where k_B is the Boltzmann constant and T is the tip or sample temperature, and

$$X_{\text{lock-in}}(V) = \begin{cases} \frac{2\sqrt{V_{\text{mod}}^2 - V^2}}{\pi V_{\text{mod}}^2}, & \text{if } |V| \leq V_m \\ 0, & \text{otherwise} \end{cases} \quad (C2)$$

the latter to account for the modulation broadening [50], where V_{mod} is the modulation amplitude. For the temperature, we used the effective temperature $T_{\text{eff}} \approx 157$ mK of the Jülich Quantum Microscope [21].

Note that for all measurements we operated the adiabatic demagnetization refrigerator (ADR) in single-shot mode, i.e., we reduced the external magnetic field to zero and allowed the experimental temperature to warm up slowly from 30 mK.

In this mode there are no additional stray fields in the sample region from the cooling pill or the ADR magnet [21]. Nevertheless, we sometimes still have remanence magnetization from the sample magnet due to the magnetic flux caught by one of the superconducting coils during the ADR run. This remanence magnetization is typically of the order of a few milliteslas and has been determined by measurements of the superconducting gap in Al [51]. Since we do not observe any change in the Kondo resonance up to ≈ 100 mT [see Fig. 2(a)], the few-millitesla offset has no detectable effect on the shape of the Kondo peak. As soon as the sample magnet is energized, the residual magnetization disappears. Therefore no additional offset has to be taken into account for magnetic-field-dependent measurements, such as the determination of the critical field B_C .

-
- [1] P. Willke, W. Paul, F. D. Natterer, K. Yang, Y. Bae, T. Choi, J. Fernández-Rossier, A. J. Heinrich, and C. P. Lutz, Probing quantum coherence in single-atom electron spin resonance, *Sci. Adv.* **4**, eaaq1543 (2018).
- [2] A. J. Heinrich, J. A. Gupta, C. P. Lutz, and D. M. Eigler, Single-atom spin-flip spectroscopy, *Science* **306**, 466 (2004).
- [3] K. Yang, W. Paul, S.-H. Phark, P. Willke, Y. Bae, T. Choi, T. Esat, A. Ardavan, A. J. Heinrich, and C. P. Lutz, Coherent spin manipulation of individual atoms on a surface, *Science* **366**, 509 (2019).
- [4] P. Willke, T. Bilgeri, X. Zhang, Y. Wang, C. Wolf, H. Aubin, A. Heinrich, and T. Choi, Coherent spin control of single molecules on a surface, *ACS Nano* **15**, 17959 (2021).
- [5] L. M. Veldman, L. Farinacci, R. Rejali, R. Broekhoven, J. Gobeil, D. Coffey, M. Ternes, and A. F. Otte, Free coherent evolution of a coupled atomic spin system initialized by electron scattering, *Science* **372**, 964 (2021).
- [6] A. A. Khajetoorians, D. Wegner, A. F. Otte, and I. Swart, Creating designer quantum states of matter atom-by-atom, *Nat. Rev. Phys.* **1**, 703 (2019).
- [7] K. Yang, S.-H. Phark, Y. Bae, T. Esat, P. Willke, A. Ardavan, A. J. Heinrich, and C. P. Lutz, Probing resonating valence bond states in artificial quantum magnets, *Nat. Commun.* **12**, 993 (2021).
- [8] Y. He, S. K. Gorman, D. Keith, L. Kranz, J. G. Keizer, and M. Y. Simmons, A two-qubit gate between phosphorus donor electrons in silicon, *Nature (London)* **571**, 371 (2019).
- [9] J. Kondo, Resistance minimum in dilute magnetic alloys, *Prog. Theor. Phys.* **32**, 37 (1964).
- [10] K. G. Wilson, The renormalization group: Critical phenomena and the Kondo problem, *Rev. Mod. Phys.* **47**, 773 (1975).
- [11] M. Ternes, A. J. Heinrich, and W.-D. Schneider, Spectroscopic manifestations of the Kondo effect on single adatoms, *J. Phys.: Condens. Matter* **21**, 053001 (2009).
- [12] Y.-H. Zhang, S. Kahle, T. Herden, C. Stroh, M. Mayor, U. Schlickum, M. Ternes, P. Wahl, and K. Kern, Temperature and magnetic field dependence of a Kondo system in the weak coupling regime, *Nat. Commun.* **4**, 2110 (2013).
- [13] L. Garnier, B. Verlhac, P. Abufager, N. Lorente, M. Ormaza, and L. Limot, The Kondo effect of a molecular tip as a magnetic sensor, *Nano Lett.* **20**, 8193 (2020).
- [14] T. Frauhammer, H. Chen, T. Balashov, G. Derenbach, S. Klyatskaya, E. Moreno-Pineda, M. Ruben, and W. Wulfhekel, Indirect Spin-Readout of Rare-Earth-Based Single-Molecule Magnet with Scanning Tunneling Microscopy, *Phys. Rev. Lett.* **127**, 123201 (2021).
- [15] W. Paul, K. Yang, S. Baumann, N. Romming, T. Choi, C. Lutz, and A. Heinrich, Control of the millisecond spin lifetime of an electrically probed atom, *Nat. Phys.* **13**, 403 (2017).
- [16] F. D. Natterer, K. Yang, W. Paul, P. Willke, T. Choi, T. Greber, A. J. Heinrich, and C. P. Lutz, Reading and writing single-atom magnets, *Nature (London)* **543**, 226 (2017).
- [17] A. F. Otte, M. Ternes, K. von Bergmann, S. Loth, H. Brune, C. P. Lutz, C. F. Hirjibehedin, and A. J. Heinrich, The role of magnetic anisotropy in the Kondo effect, *Nat. Phys.* **4**, 847 (2008).
- [18] K. Yang, P. Willke, Y. Bae, A. Ferrón, J. L. Lado, A. Ardavan, J. Fernández-Rossier, A. J. Heinrich, and C. P. Lutz, Electrically controlled nuclear polarization of individual atoms, *Nat. Nanotechnol.* **13**, 1120 (2018).
- [19] S. M. Cronenwett, T. H. Oosterkamp, and L. P. Kouwenhoven, A tunable Kondo effect in quantum dots, *Science* **281**, 540 (1998).
- [20] W. G. van der Wiel, S. D. Franceschi, T. Fujisawa, J. M. Elzerman, S. Tarucha, and L. P. Kouwenhoven, The Kondo effect in the unitary limit, *Science* **289**, 2105 (2000).
- [21] T. Esat, P. Borgens, X. Yang, P. Coenen, V. Cherepanov, A. Raccanelli, F. S. Tautz, and R. Temirov, A millikelvin scanning tunneling microscope in ultra-high vacuum with adiabatic demagnetization refrigeration, *Rev. Sci. Instrum.* **92**, 063701 (2021).
- [22] T. Esat, N. Friedrich, F. S. Tautz, and R. Temirov, A standing molecule as a single-electron field emitter, *Nature (London)* **558**, 573 (2018).
- [23] M. Knol, H. H. Arefi, D. Corken, J. Gardner, F. S. Tautz, R. J. Maurer, and C. Wagner, The stabilization potential of a standing molecule, *Sci. Adv.* **7**, eabj9751 (2021).
- [24] H. H. Arefi, D. Corken, F. S. Tautz, R. J. Maurer, and C. Wagner, Design principles for metastable standing molecules, *J. Phys. Chem. C* **126**, 6880 (2022).
- [25] C. R. Ast, B. Jäck, J. Senkpiel, M. Eltschka, M. Etzkorn, J. Ankerhold, and K. Kern, Sensing the quantum limit in

- scanning tunnelling spectroscopy, *Nat. Commun.* **7**, 13009 (2016).
- [26] R. Temirov, M. F. B. Green, N. Friedrich, P. Leinen, T. Esat, P. Chmielniak, S. Sarwar, J. Rawson, P. Kögerler, C. Wagner, M. Rohlfing, and F. S. Tautz, Molecular Model of a Quantum Dot Beyond the Constant Interaction Approximation, *Phys. Rev. Lett.* **120**, 206801 (2018).
- [27] R. Žitko, R. Peters, and T. Pruschke, Splitting of the Kondo resonance in anisotropic magnetic impurities on surfaces, *New J. Phys.* **11**, 053003 (2009).
- [28] T. A. Costi, Kondo Effect in a Magnetic Field and the Magnetoresistivity of Kondo Alloys, *Phys. Rev. Lett.* **85**, 1504 (2000).
- [29] T. Esat, T. Deilmann, B. Lechtenberg, C. Wagner, P. Krüger, R. Temirov, F. B. Anders, M. Rohlfing, and F. S. Tautz, Transferring spin into an extended π orbital of a large molecule, *Phys. Rev. B* **91**, 144415 (2015).
- [30] H. O. Frota, Shape of the Kondo resonance, *Phys. Rev. B* **45**, 1096 (1992).
- [31] R. Temirov, A. Lassise, F. B. Anders, and F. S. Tautz, Kondo effect by controlled cleavage of a single-molecule contact, *Nanotechnology* **19**, 065401 (2008).
- [32] C. Toher, R. Temirov, A. Greuling, F. Pump, M. Kaczmarek, G. Cuniberti, M. Rohlfing, and F. S. Tautz, Electrical transport through a mechanically gated molecular wire, *Phys. Rev. B* **83**, 155402 (2011).
- [33] A. Greuling, M. Rohlfing, R. Temirov, F. S. Tautz, and F. B. Anders, *Ab initio* study of a mechanically gated molecule: From weak to strong correlation, *Phys. Rev. B* **84**, 125413 (2011).
- [34] A. Greuling, R. Temirov, B. Lechtenberg, F. B. Anders, M. Rohlfing, and F. S. Tautz, Spectral properties of a molecular wire in the Kondo regime, *Phys. Status Solidi B* **250**, 2386 (2013).
- [35] M. Žonda, O. Stetsovych, R. Korytár, M. Ternes, R. Temirov, A. Raccanelli, F. S. Tautz, P. Jelínek, T. Novotný, and M. Švec, Resolving ambiguity of the Kondo temperature determination in mechanically tunable single-molecule Kondo systems, *J. Phys. Chem. Lett.* **12**, 6320 (2021).
- [36] F. Eickhoff, E. Kolodzeiski, T. Esat, N. Fournier, C. Wagner, T. Deilmann, R. Temirov, M. Rohlfing, F. S. Tautz, and F. B. Anders, Inelastic electron tunneling spectroscopy for probing strongly correlated many-body systems by scanning tunneling microscopy, *Phys. Rev. B* **101**, 125405 (2020).
- [37] J. Appelbaum, “ $s - d$ ” Exchange Model of Zero-Bias Tunneling Anomalies, *Phys. Rev. Lett.* **17**, 91 (1966).
- [38] P. W. Anderson, Localized Magnetic States and Fermi-Surface Anomalies in Tunneling, *Phys. Rev. Lett.* **17**, 95 (1966).
- [39] J. A. Appelbaum, Exchange Model of Zero-Bias Tunneling Anomalies, *Phys. Rev.* **154**, 633 (1967).
- [40] M. Ternes, Spin excitations and correlations in scanning tunneling spectroscopy, *New J. Phys.* **17**, 063016 (2015).
- [41] E. Wolf and D. Losee, g -shifts in the “ s - d ” exchange theory of zero-bias tunneling anomalies, *Phys. Lett. A* **29**, 334 (1969).
- [42] K. Yang, W. Paul, F. D. Natterer, J. L. Lado, Y. Bae, P. Willke, T. Choi, A. Ferrón, J. Fernández-Rossier, A. J. Heinrich, and C. P. Lutz, Tuning the Exchange Bias on a Single Atom from 1 mT to 10 T, *Phys. Rev. Lett.* **122**, 227203 (2019).
- [43] B. Verlhac, N. Bachelier, L. Garnier, M. Ormaza, P. Abufager, R. Robles, B. M.-L., M. Ternes, N. Lorente, and L. Limot, Atomic-scale spin sensing with a single molecule at the apex of a scanning tunneling microscope, *Science* **366**, 623 (2019).
- [44] G. Czup, P. J. Wagner, F. Xue, L. Gu, J. Li, J. Yao, R. Wu, and W. Ho, Probing and imaging spin interactions with a magnetic single-molecule sensor, *Science* **364**, 670 (2019).
- [45] M. Ternes, C. P. Lutz, A. J. Heinrich, and W.-D. Schneider, Sensing the Spin of an Individual Ce Adatom, *Phys. Rev. Lett.* **124**, 167202 (2020).
- [46] C. Wagner, M. F. B. Green, P. Leinen, T. Deilmann, P. Krüger, M. Rohlfing, R. Temirov, and F. S. Tautz, Scanning Quantum Dot Microscopy, *Phys. Rev. Lett.* **115**, 026101 (2015).
- [47] C. Wagner, M. F. B. Green, M. Maiworm, P. Leinen, T. Esat, N. Ferri, N. Friedrich, R. Findeisen, A. Tkatchenko, R. Temirov, and F. S. Tautz, Quantitative imaging of electric surface potentials with single-atom sensitivity, *Nat. Mater.* **18**, 853 (2019).
- [48] *Single Charge Tunneling: Coulomb Blockade Phenomena in Nanostructures*, edited by H. Grabert and M. H. Devoret, NATO Science Series, Vol. 294 (Springer, New York, 2013).
- [49] J. Senkpiel, J. C. Klöckner, M. Etzkorn, S. Dambach, B. Kubala, W. Belzig, A. L. Yeyati, J. C. Cuevas, F. Pauly, J. Ankerhold, C. R. Ast, and K. Kern, Dynamical Coulomb Blockade as a Local Probe for Quantum Transport, *Phys. Rev. Lett.* **124**, 156803 (2020).
- [50] M. Gruber, A. Weismann, and R. Berndt, The Kondo resonance line shape in scanning tunnelling spectroscopy: instrumental aspects, *J. Phys.: Condens. Matter* **30**, 424001 (2018).
- [51] T. Esat, X. Yang, F. Mustafayev, H. Soltner, F. S. Tautz, and R. Temirov, Determining the temperature of a millikelvin scanning tunnelling microscope junction, *Commun. Phys.* **6**, 81 (2023).